CAESAR - A high-efficiency CsI(Na) scintillator array for in-beam γ-ray spectroscopy with fast rare-isotope beams

D. Weisshaar [a] A. Gade [a,b] T. Glasmacher [a,b] G. F. Grinyer [a]
D. Bazin [a] P. Adrich [a] T. Baugher [a,b] J. M. Cook [a,b]
C. Aa. Diget [a] S. McDaniel [a,b] A. Ratkiewicz [a,b] K. P. Siwek [a,b]
K. A. Walsh [a,b]

[a] *National Superconducting Cyclotron Laboratory, Michigan State University, East Lansing, MI 48824*

[b] *Department of Physics and Astronomy, Michigan State University, East Lansing, MI 48824*

Abstract

We report on the construction and commissioning of the high-efficiency CAESium-iodide scintillator ARray CAESAR, a device designed for in-beam γ-ray spectroscopy experiments utilizing fast beams of rare isotopes at the National Superconducting Cyclotron Laboratory (NSCL) at Michigan State University (MSU). CAESAR consists of 192 CsI(Na) crystals, totaling 290 kg of active scintillator material. For 1 MeV γ rays, a full-energy-peak efficiency of 35% is achieved at an in-beam energy resolution of better than 10% FWHM after event-by-event Doppler reconstruction of the γ rays emitted by nuclei moving with velocities of $v/c \sim 0.3$ – 0.4. The spectral quality of the array allows for the identification of γ-ray transi-

tions with intensities of several 10 counts in the full-energy peak and thus opens new avenues for the study of the most exotic nuclei available at the NSCL for in-beam spectroscopy.

Key words: CsI(Na) scintillator, in-beam γ-ray spectroscopy, rare-isotope beams
PACS: 29.40.Mc, 29.40.Gx, 29.30.Kv

1 Introduction

Over the past decade, the properties of short-lived, rare isotopes, dubbed "exotic nuclei", have merged into a major focus of experimental nuclear structure research. Many of the most exotic nuclear species can be produced efficiently by projectile fragmentation of energetic (100 MeV/u – GeV/u) stable beams [1,2] or in-flight fission of ^{238}U [3]. The produced rare isotopes are then available for experiments as radioactive ion beams with velocities typically exceeding 30% of the speed of light. Experiments with fast beams allow the use of thick reaction targets and provide luminosities sufficient to perform sensitive experiments at rates of only a few ions per second. For example, intermediate-energy Coulomb excitation of the projectile [4] has been developed into a powerful tool that enables a quantitative measure of collective properties of exotic nuclei and one- and two-nucleon knockout reactions [5] provide the complementary information on their single-particle structure. The in-beam spectroscopy of γ rays emitted by the reacted nuclei at velocities $v/c \geq 0.3$ has emerged as a powerful precision technique to tag the inelastic process and identify the final states populated in nuclear reactions [6]. In-beam γ-ray

* Corresponding author.
Email address: weisshaar@nscl.msu.edu (D. Weisshaar).

spectroscopy programs in this velocity regime have been initiated more than a decade ago at GANIL (France) [7], RIKEN (Japan) [8], NSCL (US) [9], and GSI (Germany) [10].

High-purity germanium (HPGe) is still the material of choice for the construction of γ-ray spectrometers. Its intrinsic energy resolution of 0.2% FWHM for γ rays at 1 MeV is unmatched. Superior energy resolution not only allows for distinguishing individual γ rays in complex, dense spectra, but also affords the discrimination of weak γ-ray transitions on top of background. These arguments remain valid for the spectroscopy of nuclei at high recoil velocities ranging from few percent to several ten percent of the speed of light. However, *segmented* HPGe detectors have to be employed, where the segmentation increases the spatial granularity and reduces the Doppler broadening of the γ rays emitted by nuclei in flight by means of event-by-event Doppler reconstruction. A system optimized for experiments at low recoil velocities of v/c ≈ 0.05 is for example MINIBALL [11] at REX/ISOLDE, while the Segmented Germanium Array SeGA [12] at NSCL or GRAPE [13] at RIKEN are instances of γ-ray spectrometers designed for intermediate-energy experiments with reaction-residue recoil velocities exceeding 30% of the speed of light. EXOGAM [14, 15] at GANIL and TIGRESS [16] at TRIUMF – both arrays are based on clover detectors [17] – follow similar concepts.

All of these γ-ray spectrometers have in common that their in-beam γ-ray energy resolution is entirely dominated by Doppler broadening. This originates from the uncertainties of the detection and emission angles of the γ rays, and the uncertainty of the velocity and location of the nucleus at the time of the emission. For lower recoil velocities, the achieved in-beam energy resolution is still well below 1% FWHM. In the following, we focus the discussion on

γ-ray spectroscopy at intermediate beam energies ($v/c \geq 0.3$) and will use the example of SeGA at NSCL when comparing to HPGe arrays. As discussed in Ref. [18], the aforementioned uncertainties routinely yield in-beam energy resolutions of 3% FWHM in SeGA for typical experimental scenarios. In Ref. [18], spectroscopic properties of $LaBr_3$:Ce were investigated for in-beam γ-ray spectroscopy at intermediate beam energies. It was concluded that a granular spectrometer built with this novel scintillator material would be a powerful replacement of HPGe spectrometers like SeGA, yielding superior timing resolution and efficiency, while still maintaining the same quality of in-beam γ-ray energy resolution. The downside of $LaBr_3$:Ce, however, is its cost which exceeds the price of other scintillator materials like NaI(Tl) by one order of magnitude, making a 4π configuration of sufficient granularity prohibitively expensive at present.

Therefore, at NSCL we have pursued the construction of a moderate-resolution, high-efficiency scintillator array that complements SeGA. Scintillators like NaI(Tl) or CsI(Na) exhibit intrinsic energy resolutions (FWHM) of approximately 7% at 1 MeV and make the design of a high-efficiency array with an energy resolution of about 10% FWHM after event-by-event Doppler reconstruction feasible. In the following, we present NSCL's CAESium iodide ARray CAESAR and describe its design and construction with the question in mind: Is it worthwhile to sacrifice a factor of three in resolution to gain an order of magnitude in efficiency?

2 Geometry of the CAESium iodide ARray CAESAR

For maximum γ-ray detection efficiency, a solid-angle coverage as close to 4π as possible was desired. The granularity of the array had to be sufficient to maintain an energy resolution of approximately 10% FWHM after Doppler reconstruction for 1 MeV γ rays emitted by reacted nuclei at velocities of $v/c = 0.4$. An additional geometrical constraint was associated with the limited space available at the pivot point – typically the reaction target position – of the S800 magnetic spectrograph required by a majority of in-beam γ-ray spectroscopy experiments at NSCL. This device is to provide event-by-event identification of reaction residues and their kinematic reconstruction. The space constraints excluded a spherical design for CAESAR, as implemented for the Crystal ball [19] and the Spin Spectrometer [20], for example, as there would not be enough space available for the forward hemisphere. However, the coverage of forward angles in fast-beam experiments is particularly important due to the forward bias of the emitted γ-ray distribution caused by the Lorentz boost.

In RIKEN's DALI and DALI2 NaI arrays [8, 21], a rectangular crystal geometry is used with the detectors arranged in concentric layers around the beam axis. Such a concept would accommodate the space constraints posed by the S800 spectrograph. The regular ordering provides a uniform efficiency response of the detectors in each layer. But this radial arrangement of rectangular crystals does not allow for close packing as the detector axes of neighboring crystals are tilted with respect to each other, leaving the solid angle between neighboring detectors effectively almost uncovered.

The arrangement and geometry of the detectors in CAESAR was guided by

results from GEANT4 [22] simulations, aiming at reaching the following goals:

- As in DALI, detectors are arranged in layers or rings perpendicular to the beam axis
- Rectangular crystal shapes were chosen with square front-face dimensions of 2" × 2" and 3" × 3". This enables the use of photomultiplier tubes with standard diameters for the most efficient and cost effective readout of the crystals
- The array has to accommodate a beam pipe of 6" diameter
- The distance between the most downstream layer and target location has to be less than 14.3", accommodating for the space constraint given by the S800 spectrograph
- The granularity of the array has to provide for each detector an energy resolution of 10% FWHM for 1 MeV γ rays emitted from the target position by a source moving at 40% of the speed of light
- The array should capitalize on nearest-neighbor addback routines. There, events measured in coincidence in two neighboring crystals are treated as a Compton scatter event and the two energies are consequently "added back"

The intrinsic energy resolution measured with a 3" NaI(Tl) detector (7.7% at 662 keV and 5.5% at 1836 keV) was implemented in the GEANT4 simulation code. The uncertainty in the velocity of the emitter due to the energy loss in the target was modeled as an equal distribution of v/c ranging from 0.38 to 0.42. This energy loss corresponds to experiments with SeGA using rather thick targets for optimizing the γ-ray yield. While this velocity uncertainty dominates already the energy resolution achievable in SeGA, its impact on energy resolution for the scintillator array is negligible.

Starting point in the simulation was a geometry made of a simple rectangular plane consisting of 56 cubic 3" crystals placed on one side of the beam pipe. The length of the detector plane along the beam direction was restricted according the spatial constraint posed by the S800 spectrograph. In the simulation, detectors placed most down- and upstream in this geometry already met the requirement for the desired in-beam energy resolution. In a next optimization step, individual detectors were allowed to retract, forming a shell around the beam pipe. In addition, the more central 3" $\times$ 3" detectors were replaced by crystals with a 2" $\times$ 2" front face to increase granularity. This improved the simulated in-beam resolution and estimated count rate for each detector. Crystals with relatively minor contribution to the detection efficiency (e.g. detectors at the corners) were removed. Finally, the optimized detector shell was mirrored to sandwich the beam pipe and the gap between both shells was filled with detectors following the same approach. In this prototype geometry, the detectors form rings perpendicular to the beam axis as shown in Fig. 1 (left). Geometries consisting of 100 to 300 crystals were investigated. The number of the detectors in the middle rings was varied, changing the diameter of the rings. The most down- and upstream rings were kept fixed, as they already provided the maximum solid-angle coverage at the extreme angles and achieved the desired energy resolution. However, a configuration with a total of 192 crystals was found to attain all of the desired goals. For a smaller number of crystals, the granularity would not have been sufficient to meet the required in-beam resolution, and adding more crystals would reduce the overlap (contact area) between neighboring rings and thus reduce efficiency and addback capability. A length of 4" for the detectors with 2" $\times$ 2" front face was found sufficient for 1 MeV γ rays. Any additional inches in length would only lead to a negligible increase in efficiency at this energy. Increasing the

length of the cubic 3" crystal would worsen their in-beam resolution, as their spatial resolution with respect to γ rays emitted from the target position is determined by their length and not by their front-face dimension.

The final design of CAESAR with 192 crystals arranged in 10 rings is shown in Fig. 1. The 6 center rings (C-H) hold 24 detectors each of 2.13" $\times$ 2.13" $\times$ 4" dimension and the two forward and two backward rings accommodate 48 3.13" $\times$ 3.13" $\times$ 3" crystals with 10 detectors placed in both rings A and J and 14 detectors in rings B and I. The slight increase in crystal size compared to the simulation was introduced for practical reasons as outlined in the next section. In this configuration, the spatial resolution of crystals of the forward and backward rings (A, B and I, J, respectively) is dominated by their length, while for crystals in the rings in between (C through H), the front faces determine the granularity.

It is worthwhile to note that, for this geometry, the impact of the gaps between crystals on the absolute efficiency is negligible as they are not radial with respect to the target position. However, because CAESAR lacks spherical symmetry, one has to rely on simulations to obtain angle-dependent in-beam detection efficiencies. With this geometry (see Fig. 1) and CsI(Na) as the detector material (see below), an energy resolution of 10% FWHM after event-by-event Doppler reconstruction and a detection efficiency exceeding 35% for 1 MeV γ rays emitted at $v/c = 40\%$ was simulated with GEANT4.

3 The CsI(Na) detectors of CAESAR

CsI(Na) was chosen as the detector material for the 192 crystals of CAESAR. Its intrinsic energy resolution, timing properties, and cost is comparable to NaI(Tl), but the material has a 30% higher stopping power for γ rays. Sample crystals of the proposed geometry from different manufacturers showed large variations in spectroscopic quality, most likely due to inhomogeneities in the light collection throughout the volume. A strong dependence of the pulse height on the depth of the interaction of the γ rays was observed. CsI(Na) crystals delivered by ScintiTech were identified to be free from these problems.

The hygroscopic CsI(Na) scintillation crystals are placed in an aluminum housing of 1 mm wall thickness. Reflective material fills the 1.5 mm gap between the crystal and the wall of the aluminum housing. The housing is sealed with a round borosilicate window. The plate that the window is glued to provides threads at the corners for a mounting flange in support of the photomultiplier tube and its housing. The photomultiplier tube with magnetic shielding and Al housing is within the envelope of the crystal enclosure and thus detectors can be placed close to each other without any gap in-between. To match the dimensions of crystal and photomultiplier housings, 0.13" was added to the crystal dimensions of nominally 3" and 2" proposed from simulations used for the design.

The spectroscopy photomultiplier tubes R1306 and R1307 from Hamamatsu are used. A passive voltage divider board distributes the externally applied positive high voltage to the dynodes. The signal is AC coupled from the an-

ode using a 4.7 μF capacitor. The photomultiplier tubes are shielded in their housings with multiple layers of μ-metal. This shielding keeps the detector assemblies operational in magnetic fields of up to 2-3 mT. Magnetic fields exceeding 0.5 mT were observed to impact the pulse height of the signals. Careful magnetic shielding is crucial for our application since the array has to be operated in the partially shielded fringe fields of the entrance quadrupole magnet of the S800 spectrograph. In light of the presence of considerable magnetic fields, alternatives to photomultiplier readout were investigated and found not to be suitable for our application. The area of a few cm^2 of photodiodes or avalanche photodiodes is too small to cover the borosilicate window and the use of light guides would reduce the photon yield by an order of magnitude. Novel silicon drift chambers can be manufactured in practical sizes, but their long collection time would hamper the timing resolution. Also their cost, in fact, presently exceeds the price of the scintillation crystals.

Each detector assembly of CAESAR was tested using an ORTEC 572 shaping amplifier connected to an 8k PC-based MCA. The detector signal was directly fed into the shaping amplifier and a shaping time constant of 10 μs was used. Smaller shaping time constants degrade the detector resolution, for example by approximately 10% at 3μs shaping time compared to 10μs. Typically, an energy resolution of 7% FWHM for ^{137}Cs irradiating the detector from the side was achieved. No detector resolution exceeded 8%. The energy resolutions measured for both crystal shapes were similar, demonstrated by the mean values of 6.7% for all 2.13" $\times$ 2.13" $\times$ 4" detectors and 7.1% for the 3.13" $\times$ 3.13" $\times$ 3" geometry. Gamma-ray energies as low as 30 keV could be detected, as was tested with the 32 keV X-ray of ^{137}Cs.

4 CAESAR electronics and data acquisition

A high speed and versatile data acquisition system has been developed for CAESAR that employs the LeCroy 4300 series of CAMAC compatible modules in which the 11-bit 4300B Fast Encoding and Readout ADCs (FERA) play a central role. The 16-channel 4300B permits rapid charge integration of incident analogue signals and conversion to digital format (11 bits in 8.5 μs) with data output on the front panel ECL port at rates of $\sim$110 ns/word. Up to 22 of these modules can be chained together and controlled using a single FERA driver (LeCroy model 4301) that is responsible for distributing conversion gates along the front panel control bus and receiving all of the data from all 4300B modules in the system via the ECL data bus. Zero and overflow suppression are also available and are essential for experiments with CAESAR where trigger event multiplicities are typically ≤ 2. Two identical branches, each consisting of 12 4300B FERA modules controlled by a single 4301 FERA driver each, are used to derive energy and timing information for the 192 detectors of CAESAR.

Raw signals directly output from the photomultiplier tubes (PMT) are first split into two branches (energy and time) using an amplifier-and-splitter board built by PicoSystems. Each board provides 16 fast amplifier circuits with fixed gain and 2$\times$16 output channels. One set of output signals (the energy branch) are first sent to a series of 12, 16-channel shaping amplifiers with fixed shaping time constants of 4 μs, which were designed and built at NSCL and available from the SeGA setup. The shaped signals are then delivered to the inputs of the 12 4300B FERA modules. The FERA modules are operated effectively as peak-sensing ADCs, where the shaped signals lasting several microseconds are only integrated over a short 25 ns time gate applied at the maximum ampli-

tude. This solution was chosen because the data acquisition for CAESAR is operated in a common start mode and conversion gates for the FERA modules are generated not earlier than 500 ns after a prompt γ-ray signal. The usage of the shaping amplifiers saved the need of 500 ns long, higher-quality delays for 192 channels between amplifier-and-splitter board output and input of the FERA module for direct charge integration.

The second set of output signals from the amplifier-and-splitter boards (the time branch) are first sent to 12 Phillips 7106 16-channel leading-edge discriminators. These modules have a common threshold for all 16 channels and were modified to include a fixed and non-extendible dead time of 1.5 μs on each channel following an over-threshold event. This was found to be necessary to avoid multiple re-triggering of the discriminator from scintillator after-pulsing. A logic OR signal from all discriminator outputs serves as a γ trigger for subsequent coincidence logic. The individual ECL output signals from the discriminators are first delayed by 500 ns using a simple cable delay made from ribbon cable of appropriate length and then sent to a set of 12, 16-channel, LeCroy 4303 time-to-FERA converters (TFC). The TFCs are operated relative to a common start generated by the master trigger and output a NIM logic signal with a width proportional to the time between the start and the stop initiated by the discriminated input signals. The NIM outputs from the TFCs are then directly input to a second series of 12 LeCroy 4300B FERA modules that integrate the TFC signal over a 500 ns gate to provide a timing measurement for each detector relative to the master trigger. The dynamic range of the TFC/FERA pair is approximately 500 ns with a dispersion of 0.25 ns per channel.

Data read out from the two FERA drivers that control the energy and time

FERAs is accomplished using two identically programmed FPGA modules (model XLM72, JTEC Instruments) that are VME compatible. These modules were programmed to provide the necessary input/output handshake with the FERA drivers and store the collected data within a 2 Mb bank of fast-access memory. Data are then read from the static RAM of the XLM72 module, inserted into the data stream, and saved to disk using standard data acquisition software packages available at NSCL.

CAESAR is usually operated in combination with advanced particle detection systems like the S800 magnetic spectrograph and particle-γ coincident events are recorded in experiments. In this configuration, CAESAR sends a prompt logic signal for each detected γ-ray event to an external coincidence electronics setup. In case of a particle-γ coincidence, a master trigger is sent back and starts the conversion of the event in CAESAR. As CAESAR is operated in a common start mode, the master trigger has to be generated within 500 ns after the prompt γ-ray trigger. The typical width of 300 ns for the particle-γ coincidence window is rather long and mainly chosen to accommodate the walk of nearly 200 ns introduced by the leading-edge discriminators used for the γ-ray timing. A walk correction performed offline in the data analysis and its ability to restore timing and suppress random coincidences will be discussed in detail in the following section.

The amplitude of the photomultiplier signals can be adjusted with the high voltage setting and provides a broad dynamic range from one MeV to several 10 MeV. Typically, a dynamic range of 8 MeV is chosen and spectroscopy of γ-ray energies down to 50 keV is feasible at this channel dispersion of 4 keV (verified with a ^{133}Ba source). Although such low thresholds are beneficial for recovering Compton scattered event in the addback mode, they are not

practical in some fast-beam experiments that produce high rates of prompt, low-energy radiation caused by atomic processes and Bremsstrahlung in the interaction of energetic projectiles with the target. Intermediate-energy or relativistic projectile Coulomb excitation experiments, which typically employ high-Z targets like Au, Bi, or Pb, are examples for such a scenario. In these cases, energy thresholds exceeding 200 keV are chosen to reduce the dead time of the data acquisition system by eliminating the low-energy coincidence triggers caused by the beam-related background.

5 Performance of CAESAR

5.1 Experimental setup

A photograph of CAESAR installed in front of the S800 spectrograph is shown in Fig. 2. In order to provide a better view at the geometry of the array, the most upstream ring (A) is completely removed and some detectors from ring B are taken out as well. The 6" beam pipe opened at its upstream end on the photograph serves as target chamber. The target is located inside the beam pipe at the pivot point of the S800 magnetic spectrograph. The target itself is located in a cradle which is pushed with a dedicated precision stick to its exact position. This target position at the spectrograph's pivot point ensures the best angle acceptance for reaction residues entering the S800. With respect to the center of CAESAR, the target is located 2.5 cm downstream, close to the center of ring F (see Fig. 1). This location is not optimal for the efficiency for γ rays emitted in flight as the Lorentz boost biases the γ-ray distribution to forward angles. However, simulations show that, compared to a target position

exactly in the center of CAESAR, the efficiency is reduced for in-flight γ rays by less than 3%.

5.2 Measurements with stationary sources

Various calibration measurements were performed with standard radioactive sources placed at the target position inside CAESAR. For some of the measurements, a high-purity germanium (HPGe) detector was added to the setup. As shown in Fig. 2, the opened beam pipe allowed to place a HPGe detector approximately in the center of ring A. This setup was used to trigger on γ-γ coincidences between the HPGe detector and CAESAR. For sources that emit coincident γ rays, e.g. ^{60}Co, ^{88}Y, and ^{22}Na, the condition of absorbing the upper γ-ray transition of a cascade in the HPGe detector implies the likely emission of the bottom transition of the cascade into CAESAR. This coincidence condition largely eliminates random room background in the so-taken CAESAR spectra. The spectrum shown in Fig. 3 is the response of CAESAR to 1.173 MeV γ-rays from a ^{60}Co source measured in coincidence with the 1.33 MeV transition detected in the HPGe detector. This spectrum and all following spectra were analyzed in nearest-neighbor addback mode. Here, energies measured in coincidence between two neighboring crystals are attributed to a Compton scattering event from one detector into a neighboring one and the γ-ray energy is recovered by adding both energies. The addback approach removes events from the Compton plateau and places them in the full-energy peak and thus increases the full-energy-peak detection efficiency and improves the peak-to-background ratio. The energy resolution of the 1.173 MeV transition was measured to be 6.2% FWHM. For comparison, the inset in Fig. 3

shows a ^{60}Co spectrum measured by CAESAR without the HPGe coincidence.

The absolute full-energy-peak efficiency of CAESAR in the energy range from 500 keV to 2 MeV, displayed in Fig. 4, was obtained from measurements with calibrated standard γ-ray sources. The peak area of free-standing γ-ray peaks in the spectra was extracted by assigning a linear background defined by regions left and right from the peak and determining the counts in the peak above this background. The absolute efficiency was calculated from the source activity, except for ^{60}Co. Here, the spectra containing a single γ ray measured in coincidence with the HPGe detector were analyzed. The yield normalized to the singles rate of the corresponding γ-ray energy measured in the HPGe detector then gives the absolute efficiency. Two efficiency curves are shown: with nearest-neighbor addback mode (dashed line) and without the addback routine (solid line). For γ-ray energies above 1 MeV, more than 20% of the intensity in the full-energy peak is recovered with the nearest-neighbor-addback approach, while above 2 MeV the relative gain in full-energy-peak efficiency exceeds 30%. The latter was extracted from spectra measured with a ^{226}Ra source. The spectrum of a ^{226}Ra source is too dense and complex for the simple approach used here for efficiency determination, but allows to extract addback factors. Fig. 4 shows that the efficiency of CAESAR exceeds 35% for 1 MeV γ rays emitted by a source at rest. In order to calculate the efficiency for γ rays emitted in-flight, effects like the Lorentz boost, Doppler shift to different energies in the laboratory system, and γ-ray angular distributions have to be taken into account. Simulations of CAESAR show that the γ-ray efficiency is reduced by less than 10% if the emitter is moving at a velocity of 0.4 c compared to emission at rest.

Fig. 8 shows the intrinsic energy resolution of CAESAR. The data points

were determined from the sum spectrum of all 192 calibrated detectors. For the detector calibration a second-order polynomial was usually sufficient, but in some cases third-order polynomials were needed to accommodate strong non-linearities of individual FERA 4300B channels. In addition to the energy resolution of the γ-ray transitions used for the efficiency determination, resolutions at 356 keV (^{133}Ba), 2.45 MeV (^{226}Ra), and 2.61 MeV (room background radiation) are given.

5.3 In-beam γ-ray spectroscopy

The in-beam response of CAESAR was characterized from experiments utilizing two types of nuclear reactions with fast ion beams: intermediate-energy Coulomb excitation of projectiles induced by a high-Z target and secondary fragmentation of a projectile beam on a beryllium target. The projectile beams were delivered by the Coupled Cyclotron Facility [23] at NSCL.

For the Coulomb excitation measurement, a primary beam of stable ^{58}Ni nuclei at 96 MeV/nucleon was scattered off a 257 mg/cm^2 thick gold target. For the secondary fragmentation experiment, a cocktail beam of neutron-rich chlorine, argon, and potassium isotopes with energies around 75 MeV/nucleon interacted with a 188 mg/cm^2 beryllium target to produce lighter, secondary fragmentation residues.

Gamma-ray events in CAESAR were measured in coincidence with particles detected by the S800 magnetic spectrograph. The trigger threshold for γ-ray events was set to 250 keV in order to reduce the prompt coincidence rate with low-energy Bremsstrahlung in the Coulomb-excitation measurement and re-

mained unchanged for the measurement with the beryllium target. The event-by-event particle identification with the S800 focal-plane detectors allowed to analyze the individual γ-ray spectra associated with the different projectile-like reaction residues emerging from the target. The γ-ray energies measured in the laboratory system were event-by-event Doppler reconstructed into the rest frame of the moving reaction residue. The parameters necessary for the reconstruction are the emission angle of the γ ray with respect to the direction of the γ-ray emitting nucleus and its velocity. Here, typically the mid-target velocity is used. Emission angles are calculated with respect to the beam axis from the position of the crystal that registered the event relative to the known target position. In case of "addback events", the measured energies are added first and are then Doppler corrected, using the position of the crystal with the largest energy deposition as indicator of the first interaction.

Incoming projectiles impinging on the reaction target were identified event-by-event by measuring their time-of-flight between fast plastic scintillators located at the exit of the A1900 fragment separator [24] and at the object position of the S800 beam line. The timing data of the fast plastic detector at the latter location, 22.4 m in front of the reaction target, also served as time reference for the γ-ray detection in the data analysis. In Fig. 5, the correlation of the γ-ray timing and energy measured in a single detector of ring E is shown in (a). This data is taken from Coulomb excitation of ^{58}Ni projectiles on the gold target The distribution of prompt γ rays and the slope of the energy-dependent walk exceeding a range of 150 ns are very apparent. For prompt γ-ray energies close to the threshold of 250 keV, the distribution in time is 100 ns wide but narrows rapidly toward higher energies. The slope can be described with a function $t(E) = a + b/(E + c) + d/E^2$ with E as the measured γ-ray energy and with

a, b, c, and d as free parameters. The parameters were determined for each individual detector from the data and the obtained functions $t(E)$ were used to correct for the walk in the offline analysis. Fig. 5 (b) shows the time-energy correlation of all detectors of ring E after applying the walk correction. At this level of statistics, the accumulation of counts at energies of 547 keV and 1230 keV and at time 50 ns become visible and corresponds to the excitation of the gold target (547 keV) and the ^{58}Ni projectiles (1454 keV, Doppler shifted to 1230 keV in ring E). The time resolution (FWHM) at those energies is 9.0 ns and 4.5 ns, respectively. The homogeneous distribution in time at 1460 keV corresponds to random coincidences with ^{40}K from natural background. The rather high amount of random coincidences is typical for experiments utilizing inelastic scattering as most of the projectiles enter the focal plane "unreacted" and open a coincidence window. For the example of ^{58}Ni, about 1-2 excited ^{58}Ni per 10^4 projectiles are expected, given an excitation cross section to the first 2^+ state of $\sigma \approx 200$ mb and a target thickness of 257 mg/cm^2. However, the hardware coincidence window of 300 ns and a count rate in CAESAR of several kHz from natural background radiation cause about the same number of random ^{58}Ni-γ coincidences.

The majority of random coincidences can be eliminated by applying a two-dimensional gate around the prompt part in the walk-corrected time-energy distribution. Fig. 5 (c) shows the γ-ray spectrum of ring E satisfying a gate condition which is 15 ns wide at 1.2 MeV, 25 ns at 500 keV, and 100 ns at threshold energy of 250 keV. While the gates at higher energies are wide enough to cover all prompt γ rays, the 100 ns gate is already cutting into prompt low-energy γ-ray events. The spectrum in Fig. 5 (d) was created as a difference between a spectrum obtained from a 1-dimensional time cut of 100 ns width for events

in ring E and the prompt spectrum. In this off-prompt γ-ray spectrum, the two prompt transitions at 547 keV and 1230 keV are not apparent anymore, while the room background at 1460 keV from random coincidences shows up prominently. The comparable intensity of the off-prompt spectrum and the prompt spectrum shows the importance of the two-dimensional energy-time gate condition for removing random coincidences.

In Fig. 6, the γ-ray spectra measured with full CAESAR for inelastic scattering of ^{58}Ni are shown. For all spectra, a two-dimensional gate in the walk-corrected time-energy distribution was applied for removing random background as described above. The γ-ray spectrum in the inset was measured in the laboratory system and the 547 keV transition emitted at rest from the de-excitation of the gold target nuclei can be seen. The top spectrum results from the same data after Doppler reconstruction. For the reconstruction, a mid-target velocity of $v/c = 0.40$ was used for the scattered ^{58}Ni projectiles. The full-energy peak at 1454 keV corresponds to the de-excitation γ-ray of the excited first 2^+ state of ^{58}Ni. This peak has an energy resolution of 9% FWHM. The bottom spectrum is the same except that only a fraction of the statistics was analyzed. The statistics used for this spectrum corresponds to 2.6 10^6 ^{58}Ni projectiles in total impinging on the target. This statistics translates into a 5-day experiment with much less than 10 particles per second incoming projectile rate and demonstrates the spectral quality for a low-statistics case in this background regime. A peak area of around 100 counts can clearly be discriminated from background and analyzed for cross section determination.

Besides inelastic scattering, other important reaction mechanisms to explore excited states of rare isotopes include secondary fragmentation, nucleon knockout, or nucleon pickup reactions induced by fast projectile beams [6]. All of

these reactions typically involve light reaction targets. Figure 7 shows γ-ray spectra in coincidence with ^{24}Mg produced in a secondary fragmentation reaction induced by a neutron-rich chlorine beam interacting with a 188 mg/cm^2 thick ^{9}Be target. The particle-γ trigger condition for these types of reactions is much more selective than for inelastic scattering, since the unreacted beam can be mostly rejected with the spectrograph. Also, a large fraction of the desired reaction residues typically is produced in excited states and thus the number of excited over detected nuclei is much more favorable than for inelastic scattering where unreacted projectiles cannot easily be discriminated. Consequently, the contribution from random coincidences is small; the events shown in Fig. 7 are prompt within the timing resolution of the scintillators. As reported in [18], the background encountered in γ-ray spectra from such reactions is, similar to Bremsstrahlung encountered with high-Z targets, prompt and can be reduced significantly only by improved timing for the γ-ray detection ($\leq$ 1 ns). The clearly visible γ-ray transitions at 1369 keV and 2754 keV originate from the decays of the first 2^+ and 4^+ state of ^{24}Mg, respectively. For the Doppler reconstruction, a mid-target velocity of $v/c = 0.35$ was used. A small fraction of the statistics was analyzed to obtain the bottom spectrum (only 360 ^{24}Mg nuclei detected in total). The 1369 keV transition with around 60 counts in the full-energy peak is clearly visible and also the 2754 keV transition is still significant. The measured energy resolutions from the Doppler-reconstructed spectra for both γ-ray transitions along with the ones from other γ-ray energies measured in coincidence with other reaction products are compiled in Fig. 8. For energies above 1 MeV, the energy resolution after Doppler-shift reconstruction is considerably better than 10% (FWHM).

6 Summary

The CAESium iodide ARray CAESAR consisting of 192 CsI(Na) crystals was successfully commissioned at the National Superconducting Cyclotron Laboratory for γ-ray spectroscopy with fast beams of rare isotopes. The array complements the existing Segmented Germanium Array (SeGA) and provides one order of magnitude higher efficiency (35% at 1 MeV) at the expense of energy resolution (10% FWHM at 1 MeV) in the Doppler-reconstructed spectra. The performance of CAESAR was investigated in two different types of measurements, Coulomb excitation with a high-Z target and ^{9}Be-induced secondary fragmentation. In the latter case, the spectral quality of CAESAR combined with the low background in the γ-ray spectra is sufficient to identify γ-ray transitions with a few ten counts in the full-energy peak. In experiments employing inelastic scattering of projectiles off high-Z targets, prompt Bremsstrahlung and other atomic processes yield significant prompt background in the γ-ray spectra. In this background regime, the trade-off in resolving power compared to HPGe detector arrays has to be carefully considered. The case presented in this paper demonstrates that Coulomb excitation experiments with cross sections above 100 mb and γ-ray energies close to or above 1 MeV are feasible if 100 counts in the full-energy peak can be expected.

7 Acknowledgement

We thank Vadim Gayshan (ScintiTech) and Michael Momayezi (Bridgeport Instruments) for pointing us to the scintillator material CsI(Na). We are grateful for discussions with David J. Morrissey (MSU) and for contributions and sup-

port from Lee G. Sobotka (WashU) and Jon Elson (WashU and Pico Systems) concerning electronics. This work was supported by the US National Science Foundation under contracts PHY-0722822 and PHY-0606007. G. F. Grinyer acknowledges support from the Natural Science and Engineering Research Council (NSERC) of Canada.

References

[1] H. Geissel, G. Münzenberg and K. Riisager, Ann. Rev. Nucl. Part. Sci. 45 (1995) 163.

[2] D. J. Morrissey and B. M. Sherrill, Philos. Trans. R. Soc. Lond. Ser. A. Math. Phys. Eng. Sci. 356 (1998) 1985.

[3] M. Bernas, C. Engelmann, P. Armbruster, S. Czajkowski, F. Ameil, C. Böckstiegel, Ph. Dessagne, C. Donzaud, H. Geissel, A. Heinz, Z. Janas, C. Kozhuharov, Ch. Miehe, G. Münzenberg, M. Pfützner, W. Schwab, C. Stephan, K. Sümmerer, L. Tassan-Got, B. Voss Phys. Lett. B 415 (1997) 111.

[4] T. Glasmacher, Ann. Rev. Part. Sci. 48 (1998) 1.

[5] P. G. Hansen and J. A. Tostevin, Annu. Rev. Nucl. Part. Sci. 53 (2003) 219.

[6] A. Gade, T. Glasmacher, Prog. Part. Nucl. Phys. 60 (2008) 161.

[7] R. Anne, D. Bazin, R. Bimbot, M. J. G. Borge, J. M. Corre, S. Dogny, H. Emling, D. Guillemaud-Mueller, P. G. Hansen, P. Hornshj, P. Jensen, B. Jonson, M. Lewitowicz , A. C. Mueller, R. Neugart, T. Nilsson, G. Nyman, F. Pougheon, M. G. Saint-Laurent, G. Schrieder, O. Sorlin, O. Tengblad, K. Wilhelmsen-Rolander, Z. Phys. A 352 (1995) 397.

[8] T. Motobayashi, Y. Ikeda, Y. Ando, K. Ieki, M. Inoue, N. Iwasa, T. Kikuchi, M. Kurokawa, S. Moriya, S. Ogawa, H. Murakami, S. Shimoura, Y. Yanagisawa, T. Nakamura, Y. Watanabe, M. Ishihara, T. Teranishi, H. Okuno, R. F. Casten, Phys. Lett. B 346 (1995) 9.

[9] H. Scheit, T. Glasmacher, B. A. Brown, J. Brown, P. D. Cottle, R. Harkewicz, M. Hellström, R. Ibbotson, J. K. Jewell, K. W. Kemper, D. J. Morrissey, M. Steiner, P. Thirolf, M. Thoennessen, Phys. Rev. Lett. 77 (1996) 3967.

[10] S. Wan, P. Reiter, J. Cub, H. Emling, J. Gerl, R. Schubart, D. Schwalm, Z. Phys. A 358 (1997) 213.

[11] J. Eberth, G. Pascovici, H. G. Thomas, N. Warr, D. Weisshaar, D. Habs, P. Reiter, P. Thirolf, D. Schwalm, C. Gund, H. Scheit, M. Lauer, P. Van Duppen, S. Franchoo, M. Huyse, R. M. Lieder, W. Gast, J. Gerl, K. P. Lieb, Prog. Part. Nucl. Phys. 46 (2001) 389.

[12] W. F. Mueller, J. A. Church, T. Glasmacher, D. Gutknecht, G. Hackman, P. G. Hansen, Z. Hu, K. L. Miller, P. Quirin, Nucl. Instr. and Meth. A 466 (2001) 492.

[13] S. Shimoura Nucl. Instr. and Meth. B 266 (2008) 4131.

[14] F. Azaiez, Nucl. Phys. A 654 (1999) 1003c.

[15] J. Simpson, F. Azaiez, G. deFrance, J. Fouan, J. Gerl, R. Julin, W. Korten, P. J. Nolan, B. M. Nyako, G. Sletten and P. M. Walker, Acta Phys. Hungarica 11 (2000) 159.

[16] H. C. Scraggs, C. J. Pearson, G. Hackman, M. B. Smith, R. A. E. Austin, G. C. Ball, A. J. Boston, P. Bricault, R. S. Chakrawarthy, R. Churchman, N. Cowan, G. Cronkhite, E. S. Cunningham, T. E. Drake, P. Finlay, P. E. Garrett, G. F. Grinyer, B. Hyland, B. Jones, J. R. Leslie, J.-P. Martin, D. Morris, A. C. Morton, A. A. Phillips, F. Sarazin, M. A. Schumaker,

C. E. Svensson, J. J. Valiente-Dobon , J. C. Waddington, L. M. Watters and L. Zimmerman, Nucl. Instr. and Meth. A 543 (2005) 431.

[17] G. Duchene, F. A. Beck, P. J. Twin, G. de France, D. Curien, L. Han, C. W. Beausang, M. A. Bentley, P. J. Nolan, and J. Simpson, Nucl. Instr. and Meth. A 432 (1999) 90.

[18] D. Weisshaar, M. S. Wallace, P. Adrich, D. Bazin, C. M. Campbell, J. M. Cook, S. Ettenauer, A. Gade, T. Glasmacher, S. McDaniel, A. Obertelli, A. Ratkiewicz, A. M. Rogers, K. Siwek and S. R. Tornga, Nucl. Instr. and Meth. A 594 (2008) 56.

[19] V. Metag, R. D. Fischer, W. Kuehn, R. Muehlhans, R. Novotny, D. Habs, U. v. Helmolt, H. W. Heyng, R. Kroth, D. Pelte, D. Schwalm, W. Hennerici, H. J. Hennrich, G. Himmele, E. Jaeschke, R. Repnow, W. Wahl, E. Adelberger, A. Lazzarini, R. S. Simon, R. Albrecht and B. Kolb, Nucl. Phys. A409 (1983) 3310.

[20] M. Jääskeläinen, D. G. Sarantites, R. Woodward, F. A. Dilmanian, J. T. Hood, R. Jääskeläinen, D. C. Hensley, M. L. Halbert and J. H. Barker, Nucl. Instr. and Meth. 204 (1983) 385.

[21] S. Takeuchi, N. Aoi, T. Motobayashi, S. Ota, E. Takeshita, H. Suzuki, H. Baba, T. Fukui, Y. Hashimoto, K. Ieki, N. Imai, H. Iwasaki, S. Kanno, Y. Kondo, T. Kubo, K. Kurita, T. Minemura, T. Nakabayashi, T. Nakamura, T. Okumura, T. K. Onishi, H. Sakurai, S. Shimoura, R. Sugou, D. Suzuki, M. K. Suzuki, M. Takashina, M. Tamaki, K. Tanaka, Y. Togano, and K. Yamada, Phys. Rev. C 79 (2009) 054319.

[22] S. Agostinelli, J. Allison, K. Amako, J. Apostolakis, H. Araujo, P. Arce, M. Asai, D. Axen, S. Banerjee, l, G. Barrand, F. Behner, L. Bellagamba, J. Boudreau, L. Broglia, A. Brunengo, H. Burkhardt, S. Chauvie, J. Chuma,

R. Chytracek, G. Cooperman, G. Cosmo, P. Degtyarenko, A. Dell'Acqua, G. Depaola, D. Dietrich, R. Enami, A. Feliciello, C. Ferguson, H. Fesefeldt G. Folger, F. Foppiano, A. Forti, S. Garelli, S. Giani, R. Giannitrapani, D. Gibin, J. J. Gmez Cadenas, I. Gonzalez, G. Gracia Abril, G. Greeniaus, W. Greiner, V. Grichine, A. Grossheim, S. Guatelli, P. Gumplinger, R. Hamatsu, K. Hashimoto, H. Hasui, A. Heikkinen, A. Howard, V. Ivanchenko, A. Johnson, F. W. Jones, J. Kallenbach, N. Kanaya, M. Kawabata, Y. Kawabata, M. Kawaguti, S. Kelner, P. Kent, A. Kimura, T. Kodama, R. Kokoulin, M. Kossov, H. Kurashige, E. Lamanna, T. Lampen, V. Lara, V. Lefebure, F. Lei, M. Liendl, W. Lockman, F. Longo, S. Magni, M. Maire, E. Medernach, K. Minamimoto, P. Mora de Freitas, Y. Morita, K. Murakami, M. Nagamatu, R. Nartallo, P. Nieminen, T. Nishimura, K. Ohtsubo, M. Okamura, S. O'Neale, Y. Oohata, K. Paech, J. Perl, A. Pfeiffer, M. G. Pia, F. Ranjard, A. Rybin, S. Sadilov, E. Di Salvo, G. Santin, T. Sasaki, N. Savvas, Y. Sawada, S. Scherer, S. Sei, V. Sirotenko, D. Smith, N. Starkov, H. Stoecker, J. Sulkimo, M. Takahata, S. Tanaka, E. Tcherniaev, E. Safai Tehrani, M. Tropeano, P. Truscott, H. Uno, L. Urban, P. Urban, M. Verderi, A. Walkden, W. Wander, H. Weber, J. P. Wellisch, T. Wenaus, D. C. Williams, D. Wright, T. Yamada, H. Yoshida and D. Zschiesche, Nucl. Instr. Meth. A 506 (2003) 250.

[23] F. Marti, P. Miller, D. Poe, M. Steiner, J. Stetson, X. Y. Wu, in: F. Marti, Editor, Proceedings of the 16th Conference on Cyclotrons and Their Applications, vol. 600, American Institute of Physics, East Lansing, MI (2001), 64.

[24] D. J. Morrissey, B. M. Sherrill, M. Steiner, A. Stolz and I. Wiedenhoever, Nucl. Instr. Meth. B 204 (2003) 90.

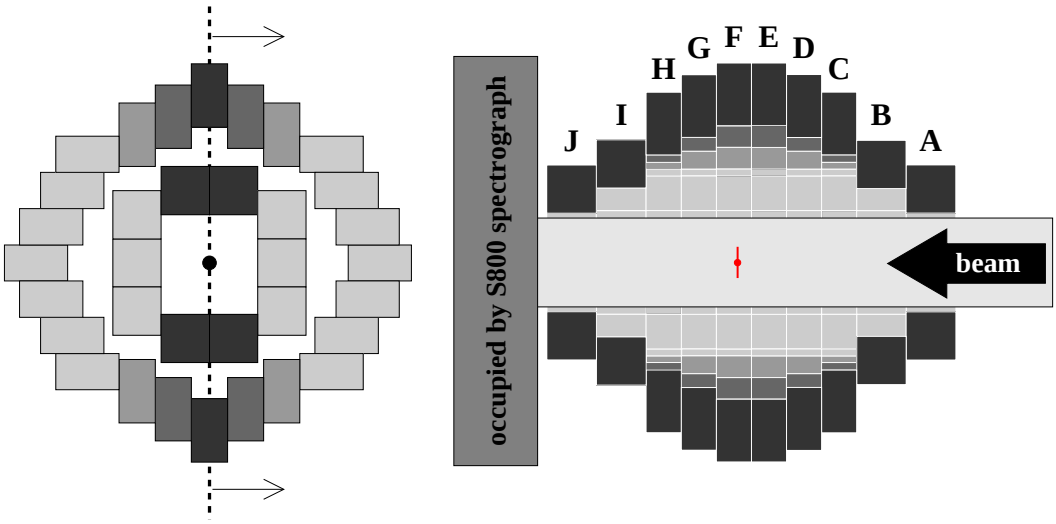

Fig. 1. The sketches show the arrangement of the 2" × 2" × 4" and 3" × 3" × 3" crystals in CAESAR. Left: Cross-sectional view perpendicular to the beam axis showing ring J and F. Right: Cross sectional view parallel to the beam axis showing the 10 rings of the array (labeled A-J) and the target position. The grey scale of the crystals corresponds to the position in the rings shown on the left.

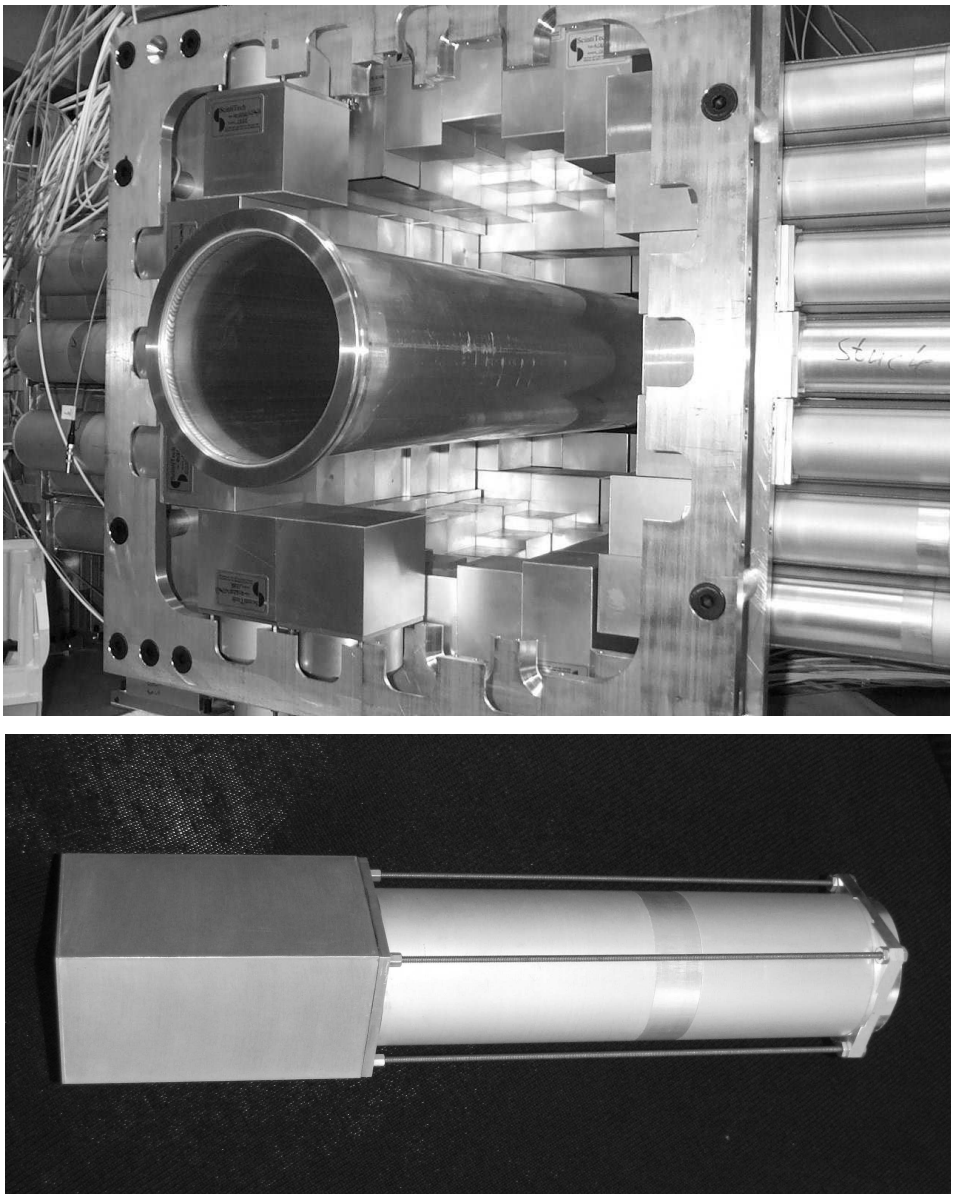

Fig. 2. The upper photograph shows the CAESAR setup in front of the S800 spectrograph. The most upstream ring A and eight 3"× 3"× 3" detectors of ring B are removed to allow a view inside of CAESAR. The target is placed in a cradle positioned inside the 6" beam pipe. The other photograph shows a 2"× 2"× 4" detector.

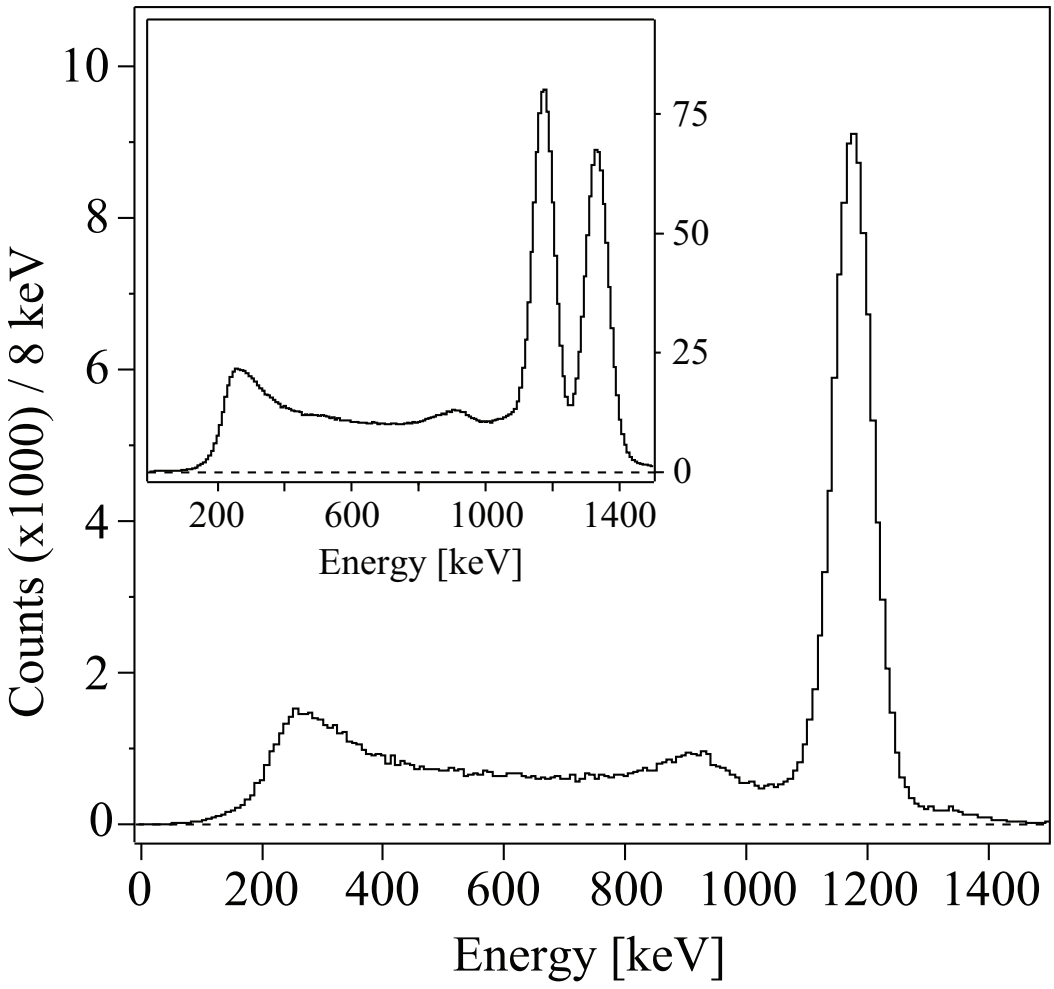

Fig. 3. Response of CAESAR to a ^{60}Co source at the target position. The spectrum was obtained in coincidences with the 1332 keV decay – the upper transition in the 1332 keV - 1173 keV coincidence cascade – measured with a HPGe detector centered within ring A of CAESAR. The inset shows the ^{60}Co spectrum without the coincidence requirement and the HPGe detector removed.

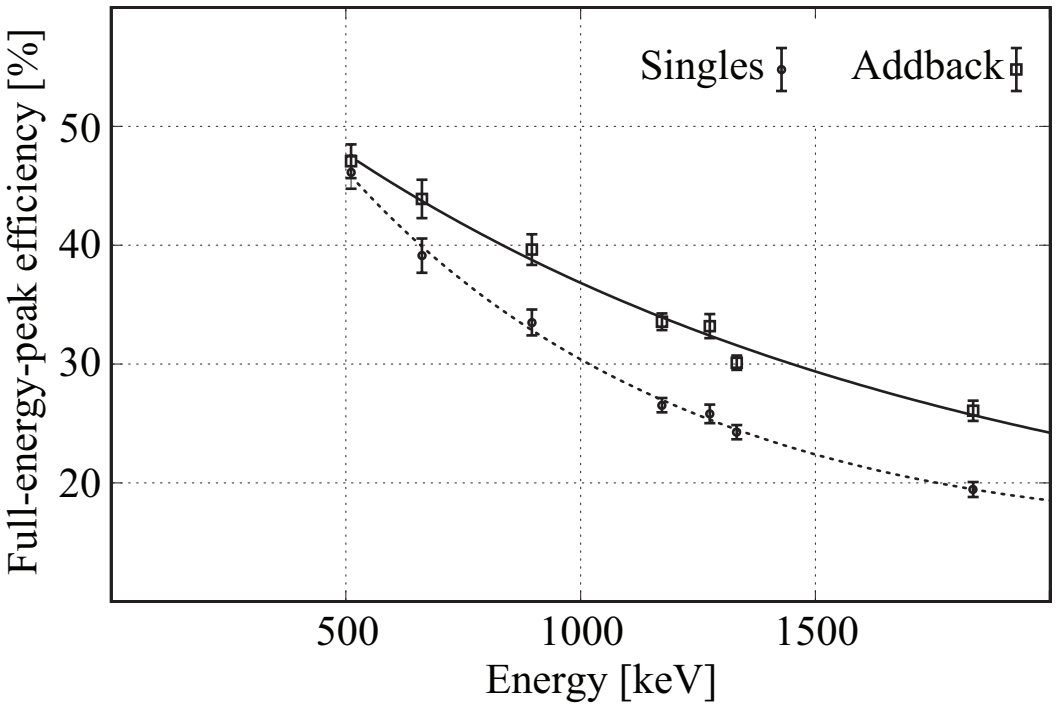

Fig. 4. Absolute full-energy-peak efficiency of CAESAR measured with standard calibration sources. Dashed line: analyzed with the nearest-neighbor addback; Solid: without addback. Both lines are to guide the eye.

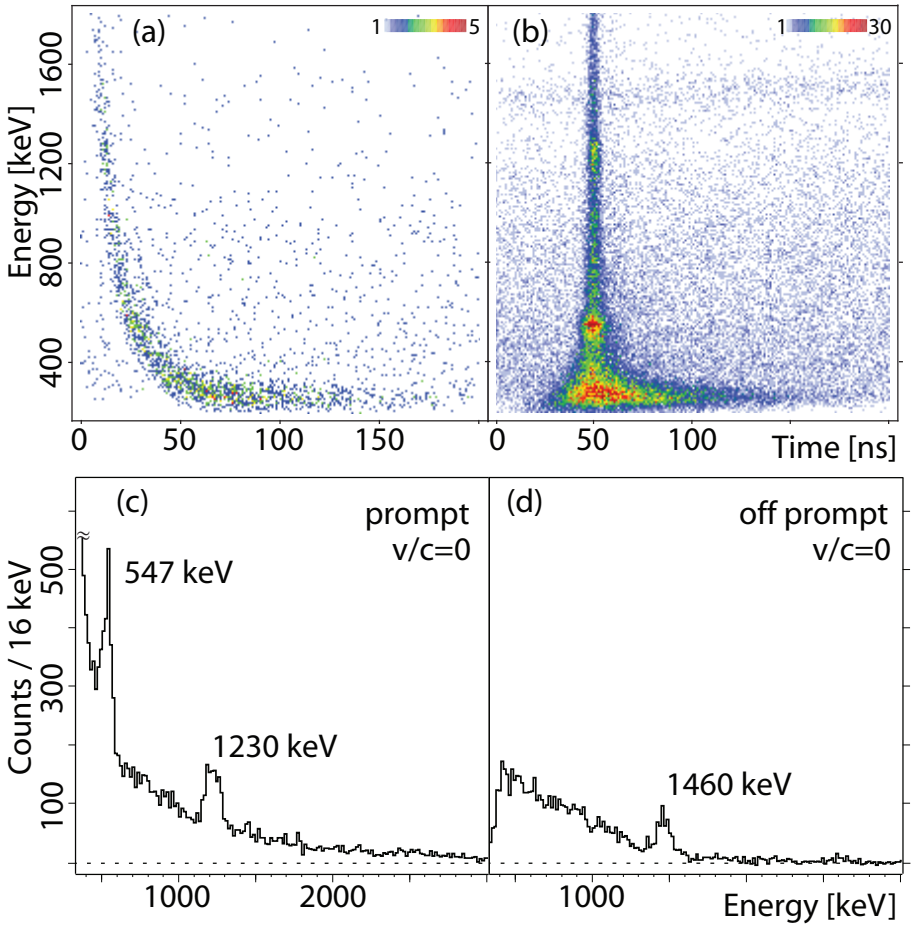

Fig. 5. (a) and (b) show the correlation between detector timing and γ-ray energy in the laboratory system for events taken in a Coulomb-excitation measurement with ^{58}Ni projectiles on a gold target. (a): The data of one detector in ring E is given without a walk correction applied. (b): Events measured in any detector in ring E are shown after walk correction. The energy spectrum shown in (c) results from applying a two-dimensional time-energy gate around the prompt events, showing the γ-ray transition from target excitation and projectile excitation (not Doppler-corrected) for all detectors of ring E. (d): Same spectrum for events outside this prompt gate. The prominent peak at 1460 keV corresponds to room background.

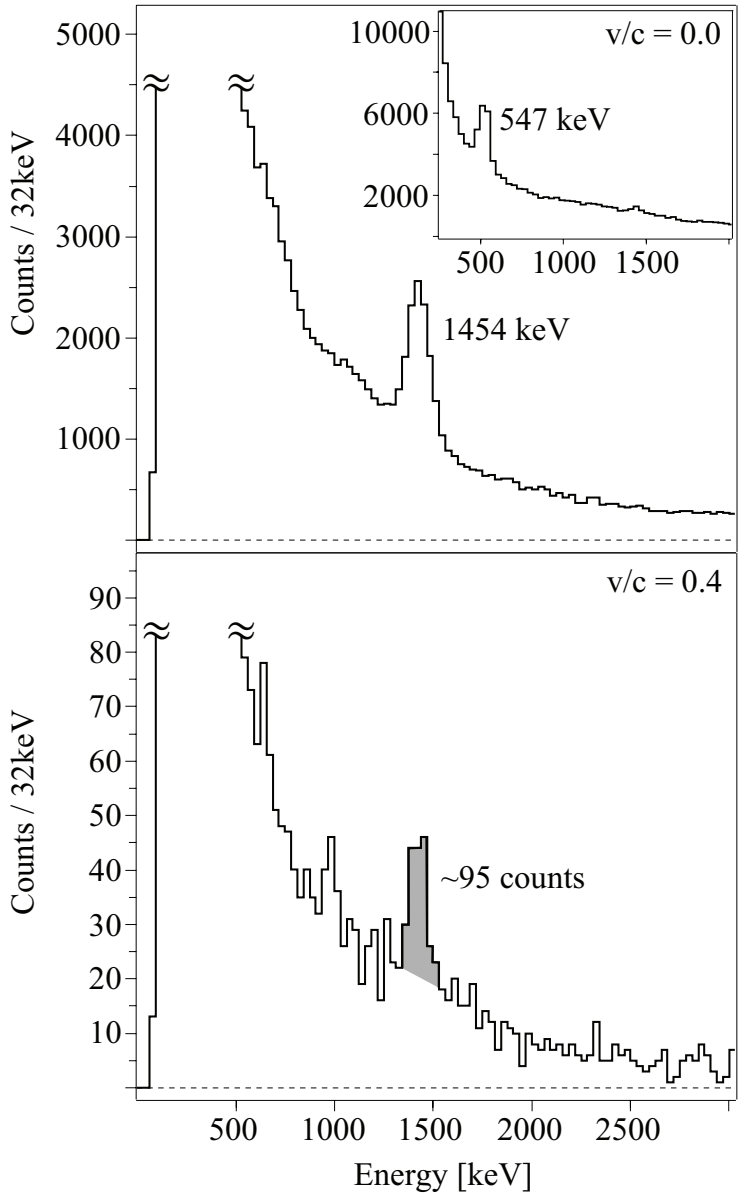

Fig. 6. Response of CAESAR to γ-ray emission in inelastic scattering of ^{58}Ni from a 257 mg/cm^2 gold target. Upper panel: Doppler-reconstructed γ-ray spectrum measured in coincidence with scattered ^{58}Ni. The 1454 keV γ-ray corresponds to the decay of the Coulomb-excited first 2^+ state of ^{58}Ni to the ground state. The inset shows the same events in the laboratory system. The excitation of the ^{197}Au target nuclei results in a peak at 547 keV. Lower panel: Same data as above, but with low statistics. This spectrum demonstrates that 100 counts in the full-energy peak are sufficient to identify a γ-ray transition in this case.

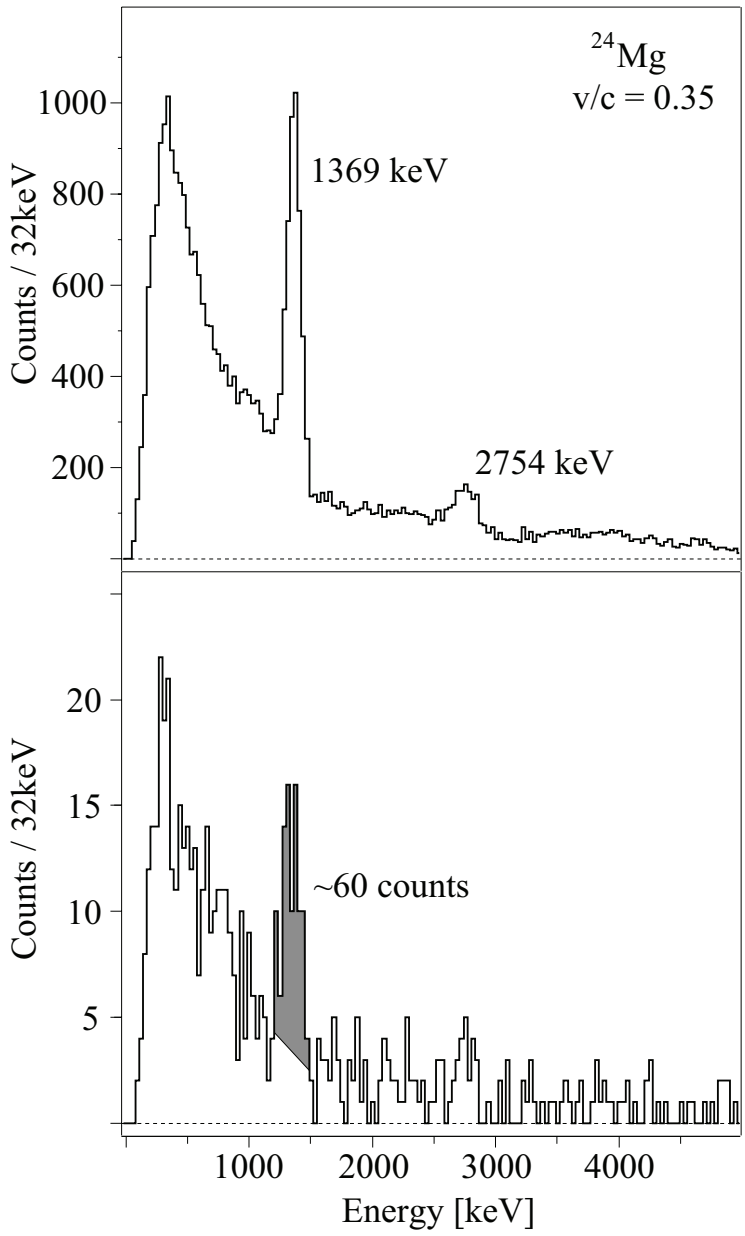

Fig. 7. Gamma-ray spectra measured in coincidence with ^{24}Mg produced by secondary fragmentation of chlorine on a 188 mg/cm^2 beryllium target. For Doppler reconstruction a mid-target velocity of $v/c = 0.35$ was used. For the spectrum in the lower panel, only a fraction of the data set was analyzed. This demonstrates the capability of CAESAR to discriminate γ-ray transitions at low statistics.

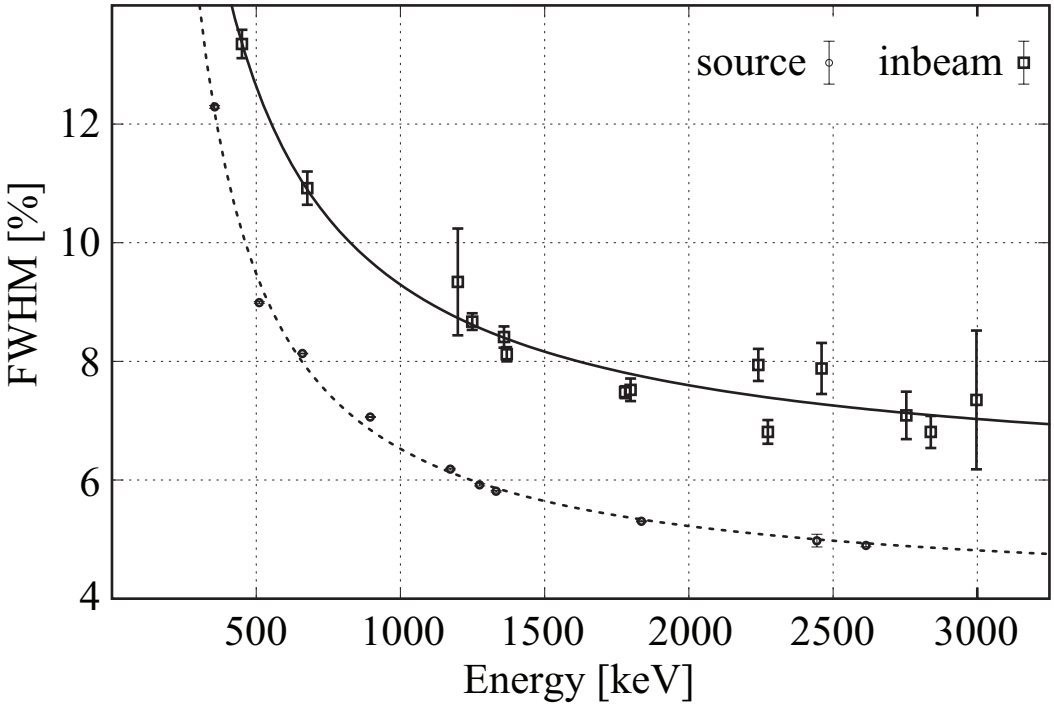

Fig. 8. In-beam energy resolutions (FWHM) and intrinsic resolution for various γ-ray energies measured with CAESAR. The in-beam energy resolutions (solid line) are obtained after Doppler reconstruction of the γ rays ($v/c = 0.35$) into the rest system. The transitions originate from various fragmentation reaction residues that were unambiguously identified in the S800 focal plane. Intrinsic resolutions were determined from standard sources. The lines stem from a fit to the function $f(E) = a + b/E + c/E^2$ and are only intended to guide the eye. The energies are given in the rest frame of the emitter.